Polymer Chemistry

ROYAL SOCIETY OF CHEMISTRY

PAPER

View Article Online
View Journal | View Issue

Cite this: *Polym. Chem.*, 2025, **16**, 4159

Long-term humid adhesion of sulfur thermoplastic polymers enabled by thioctic acid-initiated polymerization

Tongye Zhang,[a,b] Zhiyue Fang,[a,b] Shifang Luan,[a,b] Lei Wang *[a] and Hengchong Shi *[a,b]

Inverse vulcanization shows great feasibility for the utilization and conversion of sulfur by-products into high-performance sulfur-rich polymers. However, its practical application is hindered by poorly understood structural evolutions of the products and their thermodynamic instability. Herein, we develop a thioctic acid (TA)-initiated cascade polymerization strategy to synthesize thermoplastic polymers ($S_XT_YD_Z$, where *X*, *Y*, and *Z* represent the mass ratios of S_8, TA, and DIB) with controllable structural evolution and enhanced mechanical properties for humid adhesion. The key to this TA-initiated ring-opening polymerization (ROP) of sulfur is the generation of S radicals at 120 °C to produce short sulfur segments and avoid the chaotic S_1D_1 networks of traditional inverse vulcanization at high temperatures. This short sulfur structure endows $S_1T_2D_1$ with exceptional toughness (2300% strain at breaking) and hot-pressed $S_2T_1D_1$ with reinforced strength (11.64 MPa *vs.* 8.5 MPa baseline). The synergy of hydrophobic sulfur and benzene motifs and carboxyl–metal coordination bonds in $S_1T_1D_1$ ensures long-term adhesion stability (>130 days) under humid environments. We believe our work provides a foundation to balance structural control and performance in sulfur polymers, offering a scalable route to repurpose industrial sulfur waste into durable adhesives for harsh environments.

Received 2nd July 2025,
Accepted 16th August 2025

DOI: 10.1039/d5py00658a

rsc.li/polymers

1. Introduction

During the rapid development of the oil industry, sulfur has become one of the main by-products of natural gas and oil refining.[1] The global annual production of sulfur is expected to reach 90 million tons in 2028, but its consumption is far below this level. Currently, the open-air storage and disposal of excess sulfur pose various risks in terms of high cost and safety, and thus lead to many environmental concerns.[2,3] The efficient utilization of sulfur has thus garnered widespread attention due to its unique properties, including dynamic reversibility, high electrochemical capacity, and distinct optical characteristics.[4–6] Despite the great progress in sulfur-containing materials and their applications, there is still a lack of innovative strategies to harness this abundant resource effectively.[4]

As one of the most common forms of elemental sulfur (Scheme 1a), S_8 can undergo an ROP to form unstable polysulfides above 159 °C and synchronous depolymerization below this temperature in an entropy-driven and reversible manner.[7,8] Since 2011, Pyun *et al.* have initiated the direct polymerization of S_8 with unsaturated olefins as crosslinking agents to synthesize sulfur-rich polymers; this process is known as inverse vulcanization.[9] The obtained high-sulfur polymers with good solvent resistance and high electrochemical capacity can be applied in various fields, including IR imaging,[10–12] Li–S batteries,[13] and metal adsorption.[14,15] However, the production of sulfur-rich polymers *via* inverse vulcanization still faces numerous challenges at elevated polymerization temperatures (T > 170 °C), a limited variety of vinyl monomers,[5,16] and uncontrollable ring-opening of S_8. Additionally, the practical applications of inverse vulcanization products are restricted by several factors, including their poor mechanical properties, complex chain segment structures, and poor processability due to high crosslinking or high-sulfur rank (the number of S–S units in the backbone).[17] Several strategies have been proposed to solve these issues, including optimizing the ROP methods of S_8 (*e.g.*, photoinduction,[18] ball milling[19] and organocatalysis[20–23]), adjusting polymerization processes[24,25] (*e.g.*, vapor-phase synthesis[26]), controlling the rigidity of the vinyl monomer,[27,28] and introducing functional fillers[29] (*e.g.*, SiO_2,[30] polyester,[31] carbon black[32,33] and polystyrene[34]). However, the chain structure of the inverse vulcanization polymers is still unclear. Taking the typical polymer

[a]*State Key Laboratory of Polymer Science and Technology, Changchun Institute of Applied Chemistry, Chinese Academy of Sciences, Changchun 130022, P. R. China. E-mail: shihc@ciac.ac.cn, leiwang@ciac.ac.cn*
[b]*School of Applied Chemistry and Engineering, University of Science and Technology of China, Hefei 230026, P. R. China*

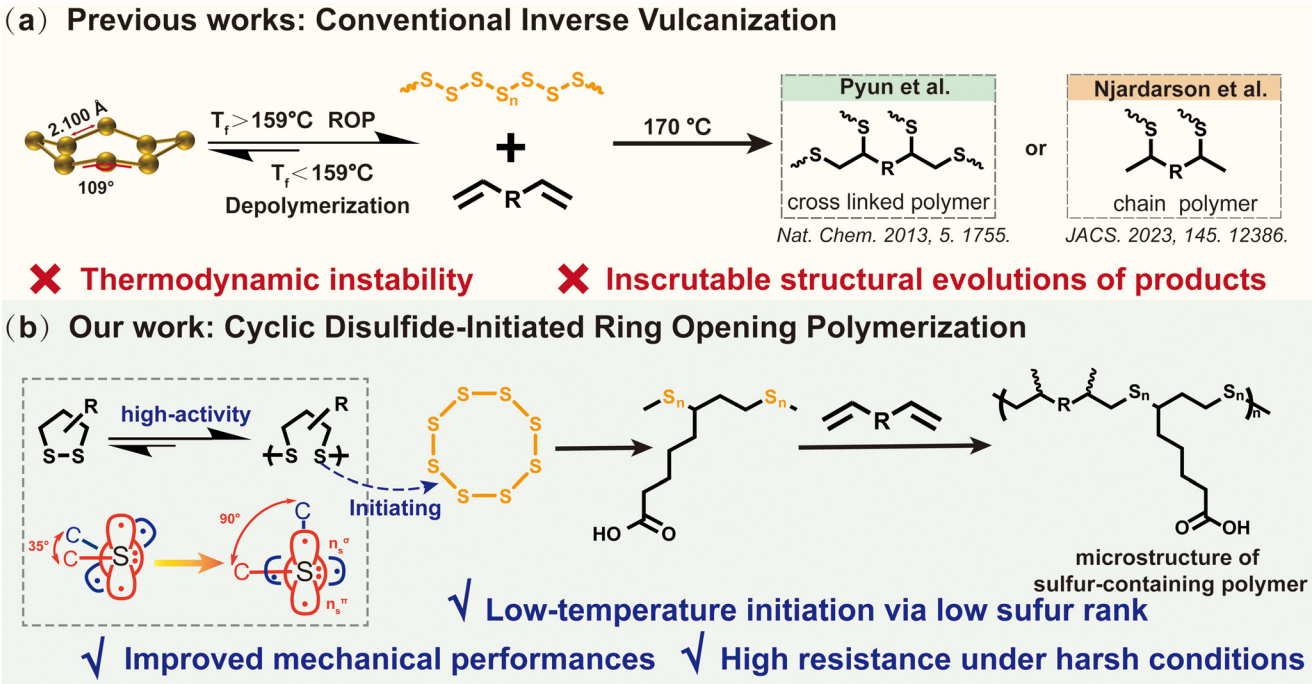

Scheme 1 Strategies for the polymerization of elemental sulfur into sulfur-containing polymers (a) Summary of previous conventional inverse vulcanization, consisting of thermal-induced S_8 ring-opening polymerization and different microstructures of polymers in 2013 and 2023. (b) The design of this work, which involves cyclic disulfide-initiated ring opening polymerization of S_8.

poly(S-r-DIB) obtained *via* the inverse vulcanization of elemental sulfur and 1,3-diisopropenylbenzene (DIB) as an example, it has widely been accepted that poly(S-r-DIB) has a complex cross-linked structure. However, the recent work reported by Pyun *et al.* indicated that the predominant repeating unit in poly(S-r-DIB) consists of thiocumyl units and the previously reported "idealized" microstructures (as shown in Scheme 1a).[35] Long-sulfur-rank polymers exhibit low modulus and poor thermal stability, while short-sulfur-rank polymers show poor toughness, high brittleness, and difficult processing.[5,36,37] Consequently, further study of the underlying mechanisms and precise regulation of the chain segments of inverse vulcanization remains imperative. As shown in Scheme 1b, tense five-membered disulfides with a -CSSC- dihedral angle of 35° and a high ring tension, facilitates the ROP by producing S radicals.[38,39] As one of the cyclic disulfides of biological source, thioctic acid (TA) can undergo the ROP polymerization to poly-TA (PTA) triggered by ROS,[40–42] low heat,[43,44] or UV light.[45–47] The presence of dynamic disulfide bonds and hydrogen bonds between carboxyl groups make TA an attractive protagonist for the design of self-healing and recyclable polymer materials.[47–50] For example, the copolymer with adjustable degradation performance was obtained by the miniemulsion polymerization of TA and *n*-butyl acrylate, which provided a new idea for the large-scale synthesis of degradable polymers in industry.[41,51,52] In addition, carboxyl groups on the PTA side chain can improve the capacity and service life of Li-S batteries *via* electrostatic interaction.[53,54] Therefore, considering the unique chemical structure of TA, it is very attractive to modify inverse vulcanization by TA. Therefore, we propose TA-initiated cascade polymerization to synthesize thermoplastic polymers ($S_XT_YD_Z$) with controllable structural evolution and enhanced mechanical properties. Concretely, TA generated sulfur radicals at 120 °C to trigger the ROP of S_8 which obtains polymers of low sulfur rank and suppresses chaotic S_1D_1 network of typical inverse vulcanization. Simultaneously, TA as a flexible polymer chain with carboxyl groups, results in the thermoplastic polymer $S_XT_YD_Z$ exhibiting superior mechanical flexibility, remarkable toughness, recycling enhancement. For example, $S_1T_2D_1$ exhibits a up to 2300% of strong tensile properties and $S_2T_1D_1$ exhibits a 37% strength increase after hot pressing (11.64 MPa *vs.* 8.5 MPa). Crucially, the carboxyl group on the side chain of $S_1T_1D_1$ polymer can form coordination bonds with metal ions, thus maintaining long-term stability under salt environments for more than 100 days (Scheme 1b). The thermoplastic polymers ($S_XT_YD_Z$) with adjustable mechanical properties and adhesion properties will have broad application prospects for self-healing and adhesives.

2. Experimental

To a 20 mL glass bottle equipped with a magnetic stirrer, elemental sulfur (S_8, quality detailed below) was added, which was then heated to 150 °C in aluminum heating blocks until an orange sulfur melt was obtained. Then, a measured quantity of thioctic acid (TA) was added to the glass bottle, and the

mixture was stirred for 2 h at 150 °C until the molten liquid was cherry red and no longer cloudy. Following that, 1,3-diisopropenylbenzene (DIB, the quality detailed below) was dropped slowly into the bottle until the color of the molten liquid became dark red and the viscosity was significantly increased. The molten liquid was then immediately poured into a 153 °C PTFE mold (preheated for 1 h), stabilized for 1 h, hot-annealed, and then stable-cured for 48 h. The sample and mold were taken out of the oven, and the sample was removed. The glass plate under the mold was leveled ahead of time to prevent uneven sample curing.

3. Results and discussion

3.1 Effect of TA in initiating S_8 ring-opening

To clarify the influences of TA-initiation of the S_8 ring-opening reaction, we first studied the ROP reaction process of S_8 and TA under specific temperature conditions, monitored using Raman and electron paramagnetic resonance (EPR). As shown in Fig. S1, S2, and Table S1, S_8 is merely melted at 120 °C but cannot undergo ROP even when the reaction time is prolonged to 12 h, as proven by the unchanged Raman signal at 472 cm^{-1}. For S_8, no characteristic signal of sulfur radicals is observed when the temperature is below 120 °C, but it appears at 150 °C (Fig. S3). These results indicate that S_8 cannot undergo a ring-opening reaction to generate the radical below 120 °C. However, with TA, it can be completely opened and self-polymerized at 120 °C as shown by the significantly enhanced Raman signal of the sulfur chain located at 512 cm^{-1}, which is attributed to the presence of asymmetric/symmetrical S–S bonds (Fig. S4 and S5). Both the generation of sulfur radicals below the melting point of TA and the chemical shifts of –S–CH_2– and –S–CH– in PTA taken together confirm the successful ring opening of TA (Fig. S6 and S7).[33] Additionally, S-radical signals of TA appeared in the EPR spectrum with a *g*-factor of 2.0045 under heating at 120 °C. Once S_8 powder was added to this TA system, the TA gradually initiated the ROP of S_8 to produce more S radicals. The corresponding EPR spectrum (Fig. 1c) shows that the S-radical signals (g = 2.0045) exhibited a slight shift after the addition of S_8 powder, which could be due to the formation of S radicals after TA-induced S_8 ring opening and copolymerization.[21,55] We also recorded the phase changes of the above reaction processes using digital photos. After the complete melting of the mixture of S_8 powder and TA, an obvious phase separation was observed due to the great difference in polarity. With increasing heating, the molten liquid of S_8 and TA transitioned from a yellow and flowing state to a brown and viscous state (Fig. 1e and Table S2).[56] We extracted the molten liquid of S_8 and TA for Raman tests at regular intervals. As shown in Fig. 1d, the observed asymmetric/symmetric S–S bond stretching vibration of TA at 512 cm^{-1} shifts to the vibration of the deformed/stretched –S–S_X–S– at 473 cm^{-1}, suggesting the successful ROP of S_8.[22,57] Therefore, we can conclude that TA first undergoes ring opening and self-polymerization at 120 °C. The terminal sulfur radicals of the ring opening of TA and PTA remain active and can serve as initiators for sulfur ring opening. Finally, the sulfur radicals of TA or PTA successfully initiate the eight-membered ring opening of S_8 powder at 120 °C (Fig. 1a).

3.2 Role of TA in regulating chain segments in inverse vulcanization

Subsequently, we studied the effect of TA in regulating the chain segments in inverse vulcanization *via* various model reactions (Schemes S1–S3), including the polymers poly(S_8-TA) (referred to as STA), poly(S_8-TA-styrene) and poly(S_8-styrene). Among the polymers poly-S_8, PTA and STA, it is interesting that the copolymer STA can be maintained at room temperature for more than six hours, while PTA begins to crystallize and precipitate within 10 min and poly-S_8 begins to depolymerize below 159 °C (Fig. 1f and S8). This can be attributed to the mutual stabilizing effect of the copolymer of S_8 and TA. We then reacted styrene with STA prepolymer at 120 °C and monitored the reaction process. EPR shows the signals of C radicals (g = 2.0015) and S radicals (g = 2.0045), and the Raman spectrum shows the disappearance of the double bond peak at 1628 cm^{-1}. These findings indicate the successful addition of styrene during the reaction. The formation of –S–S_X–S– and C–S demonstrates the successful synthesis of poly(S_8-TA-styrene) (Fig. 1g and h).

3.3 Structural analysis of poly(S_8-TA), poly(S_8-TA-styrene) and poly(S_8-styrene)

Subsequently, we conducted an in-depth structural analysis of poly(S_8-TA), poly(S_8-TA-styrene) and poly(S_8-styrene) *via* electrospray ionization mass spectrometry (ESI-MS). These three products could have different sulfur segments *via* structural control. ESI-MS confirmed that the highest sulfur rank can be identified as three for molecular weight less than 400 in mass spectrometry of poly (S_8-styrene) (Fig. S9a). However, the highest sulfur rank in poly(S_8-styrene) was calculated to be more than ten when the molecular weight exceeded 600 (Fig. S9b). The inherent instability and extensive crosslinking within the polymer could present great challenges for precise structural elucidation. This aligns with previous studies highlighting the uncontrollable nature of the ring-opening polymerization (ROP) of S_8 in conventional inverse vulcanization systems, which typically generate disordered, elongated sulfur chain architectures.[36,37] However, for STA and poly(S_8-TA-styrene), the sulfur chain segment has significantly decreased. As shown in Fig. S10, we can observe the signal peaks that reflect the structural characteristics of the polymer chain in the mass spectrum of STA. The highest sulfur rank in the STA is calculated to be five. We propose that the chemical reactivity of the sulfur chain was significantly enhanced after the TA-initiated ROP of S_8. Under such circumstances, the S-radical generated by TA can smoothly insert into the long sulfur chain and form a unique structure with alternating TA and S atoms. The insertion behavior of TA may limit the continuous growth of the sulfur chain, which is beneficial for

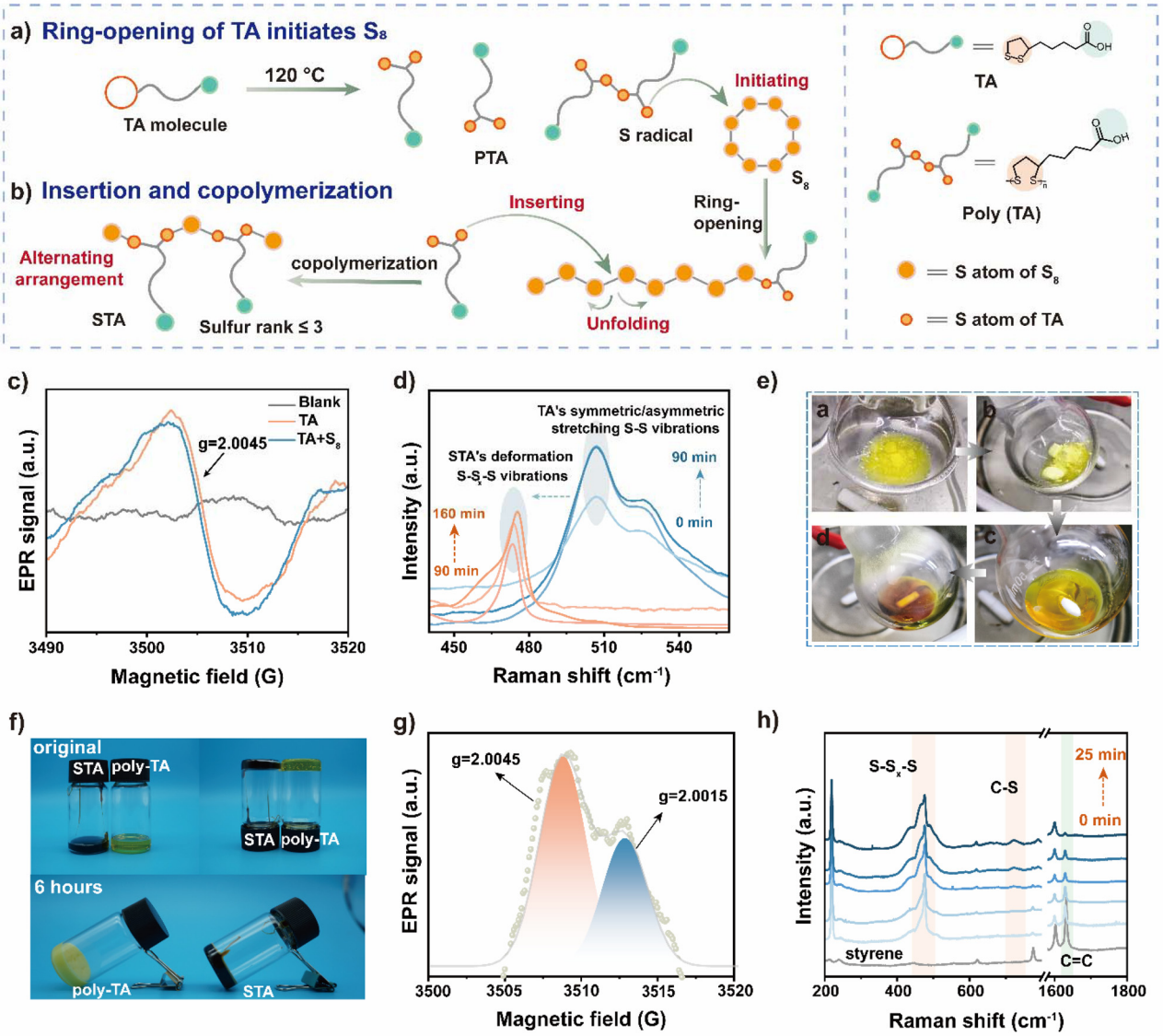

Fig. 1 TA-initiated ring opening polymerization of inverse vulcanization polymers. (a) Process of ring-opening of TA initiates S_8. (b) Insertion and copolymerization of PTA and S_8. (c) EPR spectra of TA and the mixture of TA and S_8. (d) Raman spectra of TA and the STA at variable times. (e) Monitoring the heating reaction process of TA-triggered S_8 at 120 °C. (f) Pictures of the changes in PTA and STA at room temperature. (g) EPR spectra of STA and styrene, with corresponding S and C radicals accompanied by associated curve fits. (h) Raman spectra of the STA and styrene mixture at variable times.

obtaining many short sulfur chain segments with good stability. Subsequently, we further investigated the structure of poly (S_8-TA-styrene). As shown in the mass spectrum of poly(S_8-TA-styrene) (Fig. S11), the molecular weight of the poly(S_8-TA-styrene) polymer model is also highly consistent with the experimental data, and the determined sulfur rank is about four or five. Obviously, the short sulfur rank in poly(S_8-TA-styrene), compared to the other samples, may lead to enhanced structural stability. Moreover, it also indicates that the incorporation of unsaturated styrene monomers does not affect the chain segment regulation of TA on S_8. Thus, a series of poly(S_8-TA-styrene) products with short sulfur rank are obtained *via* the regulation of the segments of poly(S_8-styrene) by TA. The detailed structural factors in Tables S3–S5 present the observed *m*/*z* values with proposed structures, accounting for the sulfur chain length. Finally, the reaction kinetics of STA and poly (S_8-TA-DIB) were studied in detail by monitoring the conversion of TA and DIB as well as the corresponding changes in molecular weight during the polymerization reaction *via* ^{1}H NMR and GPC traces (Fig. S12–20).[58] After the copolymerization of S_8 with TA, the molecular weight of STA does not increase significantly with the increase in the TA conversion rate, indicating the sulfur rank number below five is maintained well. After adding DIB, the molecular weight of poly(S_8-TA-DIB) increases promptly due to the possible formation of crosslinking sites (Fig. 1h). These results indicate

that the introduction of TA could transform the long sulfur chain structures into shorter sulfur chain segments with fewer than five sulfur atoms (Fig. 1b). It is established that TA functions both to initiate sulfur ring-opening at 120 °C and to mediate chain segment regulation through terminal sulfur radicals, resulting in structurally stabilized short-sulfur-rank polymers.

3.4 Study of structural and chain segment regulation by TA characterization

After elucidating the TA-initiated chain segment regulation, we synthesized a series of poly(S_8-TA-DIB) polymers denoted as $S_XT_YD_Z$ (where *X*, *Y*, and *Z* represent the mass ratios of S_8, TA, and DIB in the ter-polymerization), including $S_2T_1D_1$, $S_1T_1D_1$, and $S_1T_2D_1$. The subsequent structural analysis takes $S_1T_1D_1$ as an example and uses it as the representative of the experimental group. As shown in Fig. 2a, the obtained Raman spectrum of the $S_1T_1D_1$ sample reveals a significant structural transformation in comparison with its S_8, TA, and S_1T_1 controls as proven by the disappearance of the disulfide bond peak at 510 cm^{-1} for the TA monomer and the emergence of a new –S–S_X–S– peak at 470 cm^{-1}.[22,57] These observations confirm the successful ring-opening of TA and its induced copolymerization with S_8 to form polysulfide chains.[22] Additionally, as shown in the Fourier-transform infrared spectra (FT-IR) (Fig. 2b), $S_1T_1D_1$ exhibits the same C–S bond peak at 696 cm^{-1} as that of the S_1D_1 sample. Additionally, an obvious wavenumber shift is observed for the C–S bond peak from 671 cm^{-1} in TA to 696 cm^{-1} in $S_1T_1D_1$. This shift in $S_1T_1D_1$ can be attributed to the increased polarity arising from the electron-withdrawing groups on the benzene rings within the $S_1T_1D_1$ polymer structure, and the lone pair electrons on the sulfur atoms can form a weak conjugation system with the benzene rings. Furthermore, the peak at around 3350 cm^{-1} can be attributed to the O–H stretching vibration of the carboxyl groups, indicating hydrogen bonding between the $S_XT_YD_Z$ polymer chains. In addition, the vibration peak of the carboxyl group (1681 cm^{-1}) became more pronounced with increasing TA content (Fig. 2b and S21).[59,60] The appearance of the carbonyl carbon peak at 180 ppm in the ^{13}C solid-state NMR and C–H assignment in the ^{13}C–^{1}H HMQC spectrum of $S_1T_1D_1$ also confirm the ter-polymerization (Fig. S22–25). Compared with the spectrum of DIB, the disappearance of the C=C stretching vibration absorption at 1634 cm^{-1} and the CH– stretching vibration at 3087 cm^{-1} in S_1D_1 and $S_1T_1D_1$ clearly demonstrate the consumption of C=C bonds and allylic hydrogens (Fig. S26).[61] These results demonstrate the successful adduction of DIB. We performed X-ray diffraction (XRD) analysis on the $S_1T_1D_1$ sample and its S_8 and S_1D_1 controls. The broad peak located near 18° suggests that no

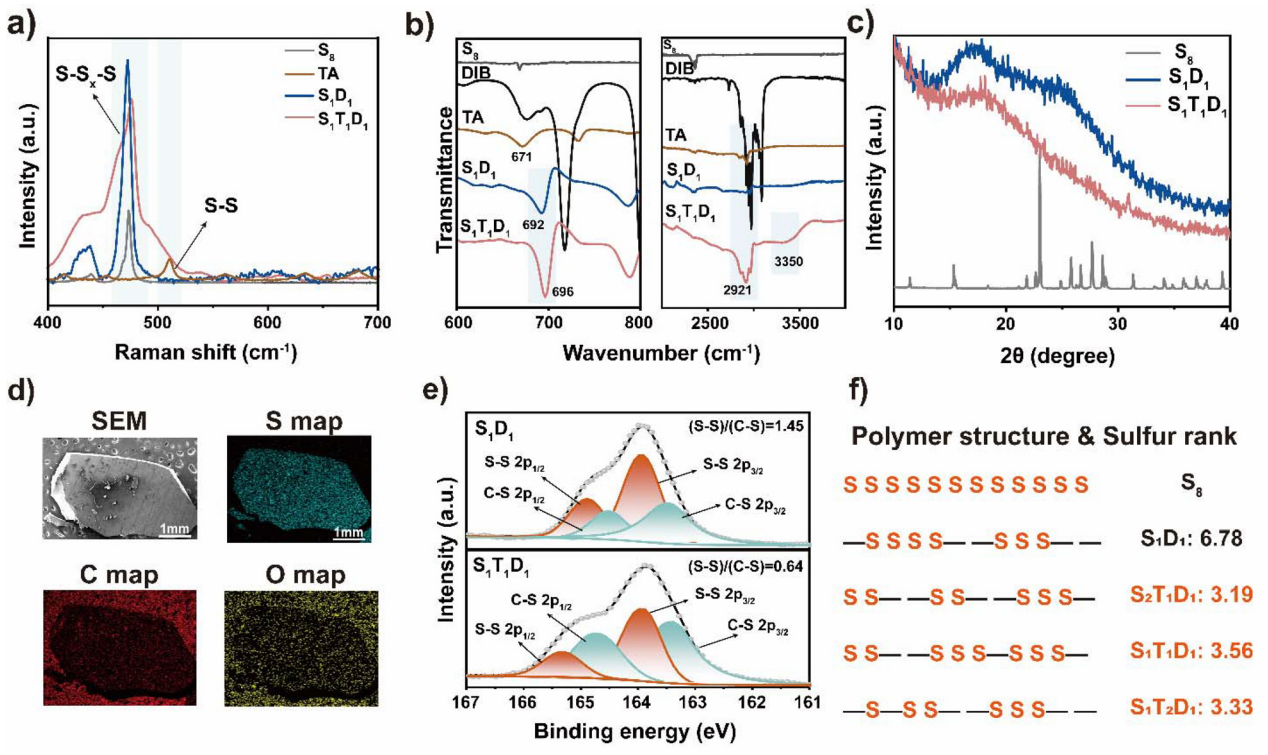

Fig. 2 Structure characterizations and sulfur rank of $S_XT_YD_Z$. (a) Raman spectra of the control S_1D_1 and of $S_1T_1D_1$ containing the monomers TA and S_8. (b) ATR FT-IR spectra of the control S_1D_1 and of $S_1T_1D_1$ containing the monomers S_8, DIB and TA. (c) XRD patterns of the control S_1D_1 and of $S_1T_1D_1$ compared to that of elemental sulfur. (d) SEM images of $S_1T_1D_1$ and its corresponding elemental mapping displayed on the right side. (e) X-ray photoelectron spectra of the control S_1D_1 and $S_1T_1D_1$. (f) Cartoon illustration of the internal structure of the control S_1D_1 and $S_XT_YD_Z$ with different ratios; "–" stands for carbon–carbon bond, and the sulfur ranks obtained by elemental analysis.

elemental sulfur exists in the as-synthesized amorphous S_1D_1 and $S_1T_1D_1$ (Fig. 2c). The uniform distribution of C, O, and S in $S_1T_1D_1$ was confirmed from scanning electron microscopy (SEM) images (Fig. 2d), suggesting the homogeneous reaction of S_8, TA, and DIB monomers.

We further explicated the segmental structures of $S_XT_YD_Z$ through X-ray photoelectron spectroscopy (XPS) and elemental analysis (EA). Both XPS and EA tests confirm a significant reduction in sulfur content after incorporating TA, indicating the successful synthesis of short-sulfur-rank polymers. The bond structure and sulfur content of S_1D_1 and $S_XT_YD_Z$ were first analyzed using XPS. As shown in Fig. 2e and Table S6, the XPS results for $S_1T_1D_1$ reveal that the S 2p peak consists of two different chemical environments at 163.48 and 164.88 eV for C–S bonds as well as at 163.98 and 165.38 eV for S–S bonds, respectively. The sulfur rank calculation is based on peak deconvolution of the S–S and C–S in the XPS data. The final ratio of S–S to C–S in the $S_1T_1D_1$ polymer is calculated to be 0.64, indicating that the average sulfur rank in the $S_1T_1D_1$ chain segments is approximately 3.56. The obtained sulfur rank of the S_1D_1 control is calculated to be 6.78 (Fig. S27, 28 and Table S7). Notably, the sulfur rank of $S_XT_YD_Z$ decreases from 6.78 to 3.56 after the introduction of TA. The sulfur contents of $S_XT_YD_Z$ determined *via* XPS show discrepancies with the theoretical feed ratios, ranging from 11.58 to 67.13 wt% (Table S8). Taking $S_2T_1D_1$ as an example, the repeated XPS measurements of the same polymer yielded sulfur content of 20.85 wt% and 35.07 wt%, indicating considerable variability and poor reproducibility of the XPS method. However, the results from EA (Table S9), provide closer values of 41.966 and 43.443 wt% for $S_2T_1D_1$. Considering the limitations of the XPS test, such as surface sensitivity and semi-quantification, the sulfur rank based on the sulfur content results from EA is more convincing.

According to previous works,[62,63] the sulfur contents obtained for the control S_1D_1 and $S_XT_YD_Z$ *via* EA can be further divided into two parts: sulfur incorporated into the polymer backbone, and sulfur not incorporated into the polymer backbone. The latter has been defined as "dark sulfur" by Tom Hasell. This so-called "dark sulfur" is distributed in the polymer matrix in an amorphous form and is regarded as an interference in the accurate calculation of the sulfur rank. Ultraviolet–visible spectroscopy (UV-Vis) was performed to test the content of dark sulfur. By establishing a standard curve based on the Beer–Lambert plot curve, the corresponding "dark sulfur" content in each as-synthesized polymer can be calculated to be 5.258 wt% for control S_1D_1, 4.091 wt% for $S_2T_1D_1$, 6.517 wt% for $S_1T_1D_1$, and 9.432 wt% for $S_1T_2D_1$ as listed in Table S10 (Fig. S29, 30 and Table S9).[62,63] Following that, the remaining polymerized sulfur contents after excluding the contributions of "dark sulfur" were calculated and are listed in Table S9. As shown in Table S10, the average sulfur rank in $S_XT_YD_Z$ and its control S_1D_1 were calculated from the EA and XPS results, and the corresponding results can be compared directly. Both the EA data and XPS data exhibit a consistent decreasing trend with the increasing TA content. Obviously, due to the semi-quantitative nature of the XPS calculation, the sulfur contents calculated *via* EA have smaller errors. For the data from EA, the sulfur rank significantly decreases from 9.95 for S_1D_1 without adding TA to a minimum of 3.02 for $S_1T_2D_1$ at the highest TA amounts. This reduction in the sulfur rank value shows a shortening of the sulfur chain length within the segment of the polymer, indicating the successful regulation of the polysulfide polymer segments by TA. The proposed probable correlations between sulfur rank and polymer structure are shown in Fig. 2f, demonstrating that TA played a critical role in regulating the chain segments in the inverse vulcanization polymers.

3.5 Thermal, mechanical properties and recycling enhancement

Excessive sulfur chain length can lead to detrimental impacts in polymer performance, manifesting as reduced mechanical properties, altered thermal stability and optical properties, increased processing difficulty, and diminished chemical resistance.[6,37] As discussed, TA modification of inverse vulcanization (control S_1D_1) effectively suppresses the growth of sulfur rank, influencing the thermal and mechanical properties of $S_XT_YD_Z$.[64,65] As shown in Fig. 3a, S31–33 and Table S11, the decomposition temperature of the $S_XT_YD_Z$ polymer is approximately 215 °C, which is 40 °C lower than that of S_1D_1. Additionally, the differential scanning calorimetry (DSC) curves reveal that as the content of the TA copolymer increases, the glass-transition temperature (T_g) gradually decreases (Fig. 3b and S34). This is attributed to PTA acting as a soft segment in the $S_XT_YD_Z$, reducing the rigidity of the polymer, thereby enhancing the flexibility of the $S_XT_YD_Z$. Hot pressing is a polymer processing technique that is commonly used as a method for recycling sulfur-containing polymers. The hot-pressing process can facilitate the rearrangement of disulfide bonds within the $S_XT_YD_Z$, resulting in the formation of a dense and uniform polymer film for investigating the mechanical properties. The stress–strain curve of $S_1T_1D_1$ with an S_8 : TA ratio of 1 : 1 indicates a maximum breaking strength of 8.5 MPa, a breaking strain of 743% and a Young's modulus of 973 MPa. With increasing TA content (S_8 : TA ratio at 1 : 2), an ultra-high strain of 2300% is achieved in the $S_1T_2D_1$ sample, but the breaking strength decreases to 1.5 MPa in comparison with the $S_1T_1D_1$ sample (Fig. 3c, d, j and Table S12). This is due to the insertion of PTA into the control S_1D_1 polysulfide chain, preventing severe chain entanglement within the $S_XT_YD_Z$. Under external stretching force, dynamic bonds in $S_XT_YD_Z$ can rapidly align and dissipate stress, thereby enabling the $S_XT_YD_Z$ to achieve high strength and high elongation. The above results can be ascribed to the incorporation of the flexible chain TA increasing the distance between polymer chains, reducing the rigidity of the S_1D_1 control, and enhancing the flexibility of $S_XT_YD_Z$. The inverse vulcanization polymer of the S_1D_1 control exhibits high brittleness both before and after hot pressing due to its high degree of crosslinking, making it difficult to process, and thus its mechanical properties could not be tested. In contrast, $S_XT_YD_Z$ polymers modified with TA

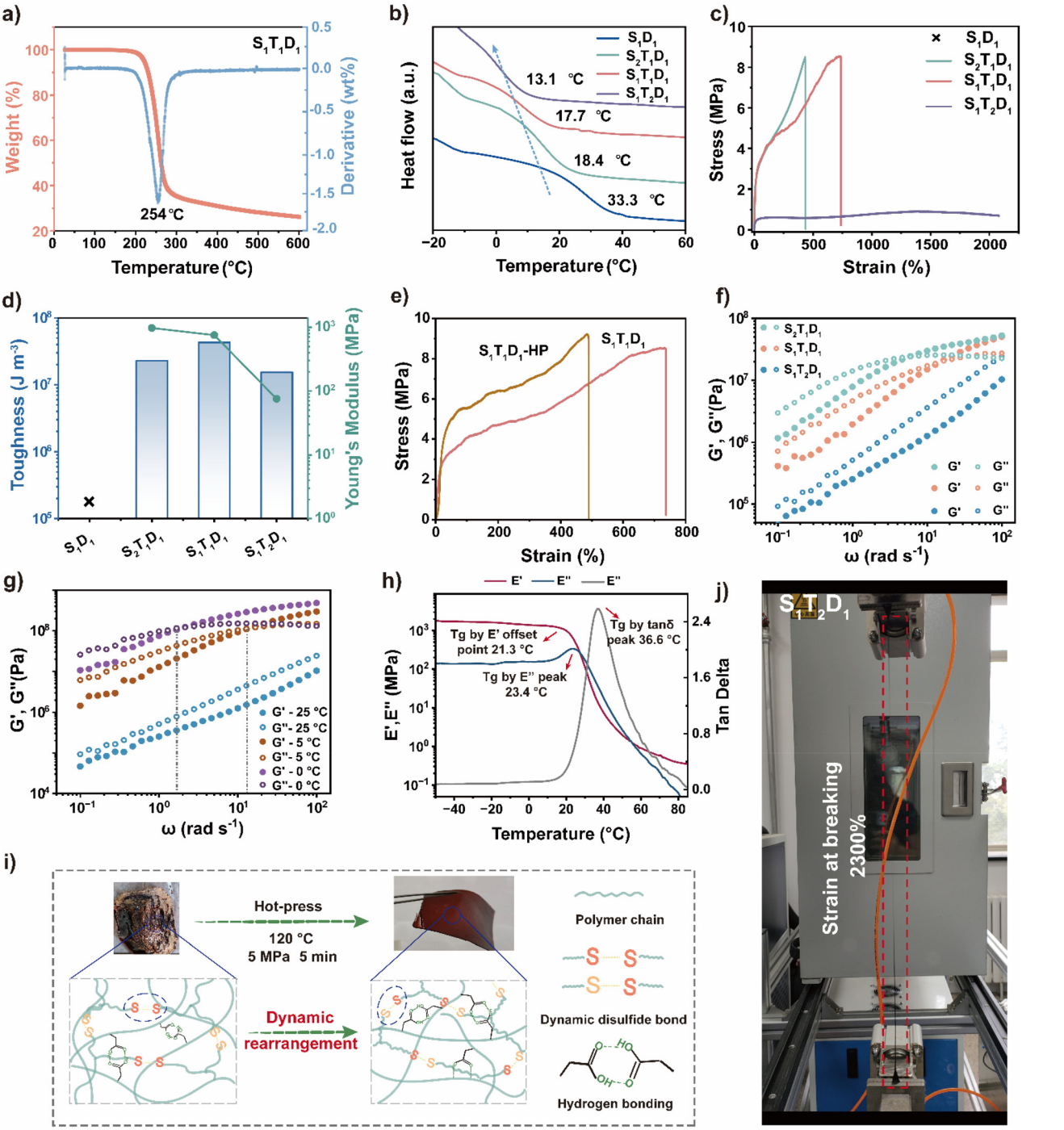

Fig. 3 Mechanical and thermal properties of $S_XT_YD_Z$. (a) TG curves of $S_1T_1D_1$, and (b) DSC curves of $S_XT_YD_Z$ and its control S_1D_1. (c) Standard stress–strain curves and (d) toughness and Young's modulus of $S_XT_YD_Z$ and its control S_1D_1. (e) Stress–strain curve of $S_1T_1D_1$ after recycling. (f) Rheological monitoring of $S_XT_YD_Z$ at 25 °C in the frequency sweep. (g) Rheological monitoring of $S_1T_2D_1$ at 25 °C, 5 °C and 0 °C in the frequency sweep. (h) Dynamic mechanical analysis of $S_1T_1D_1$. (i) Diagram illustrating the dynamic rearrangement of the disulfide bonds of $S_XT_YD_Z$ during hot pressing. (j) Photograph during the tensile test of $S_1T_2D_1$.

show good processability. The $S_XT_YD_Z$ polymers contain a significant number of S–S bonds exhibiting short sulfur rank, which is beneficial to the reprocessing. We then hot-pressed the crushed $S_XT_YD_Z$ at 90 °C under a pressure of 5 MPa for 10 min to obtain a uniform polymer ($S_XT_YD_Z$-RE), as disulfide bond activation in the linear polymer occurs at approximately 50–90 °C.[66] After conducting stress–strain tests on the polymers $S_XT_YD_Z$ and $S_XT_YD_Z$-RE, we found that the breaking

strength significantly increased after repeated hot pressing (Fig. 3e and S36). Among them, $S_2T_1D_1$ shows the most significant increase in tensile strength, rising from 8.47 MPa to 11.66 MPa (Fig. S35). To investigate the mechanisms of internal structural change during the hot-pressing process, we conducted *in situ* EPR tests on the polymer $S_1T_1D_1$ during hot pressing *via* monitoring the generation of S-radical signals (Fig. S37). We observed a prominent sulfur radical signal during the hot-pressing process of $S_1T_1D_1$, indicating the cleavage of disulfide bonds. As a result, the increase in breaking strength can be ascribed to the heat-initiated conditions causing the disulfide bonds in the $S_XT_YD_Z$ to break and rearrange continuously (Fig. 3i).[55] The solubility tests of $S_XT_YD_Z$ and $S_XT_YD_Z$-HP also show that the solubility decreases significantly and the crosslinking density increases after hot pressing (Fig. S38). This process enhances inter-chain interactions, thereby leading to improved mechanical properties. We also examined the XPS spectra of the $S_XT_YD_Z$ after hot pressing, and its sulfur rank remained less than three (Fig. S39–42 and Table S7).

To investigate the flow characteristics of $S_XT_YD_Z$, we performed dynamic rheological characterizations on $S_XT_YD_Z$. As shown in Fig. 3f, frequency sweep tests of $S_2T_1D_1$ and $S_1T_1D_1$ at 25 °C reveal a crossover point between the storage modulus (G') and loss modulus (G''). At the long timescales of low frequencies, the plateau of G' is lower than that of G'', showing viscous dissipation (liquid-like), and at the short timescales of high frequencies, the plateau of G' is higher than G'', showing a dominant elastic behavior (solid-like). In contrast, $S_1T_2D_1$ displays parallel G' and G'' curves across the entire frequency range at 25 °C, with G'' consistently higher than G' (Fig. 3f). This behavior arises from the introduction of flexible chains that lower the T_g, enabling faster molecular chain mobility and thereby enhancing viscoelasticity with liquid-like dominance. Furthermore, temperature-dependent frequency sweeps of $S_1T_2D_1$ (Fig. 3g) demonstrate a gradual increase in G' as the temperature decreased, signifying a transition from viscous to elastic behavior. The relaxation time of $S_1T_2D_1$ is further prolonged when the temperature decreases from 5 °C to 0 °C, causing the intersection point of G' and G'' to shift towards the low-frequency direction (*i.e.*, it appears "ahead of schedule"). This phenomenon reflects the suppressed thermal motion of the molecular chains at lower temperatures, which restricts segmental mobility and reinforces elastic contributions. The mechanical properties of $S_XT_YD_Z$ were also evaluated *via* dynamic mechanical analysis (DMA) tests. As expected, with increasing TA content, the loss factor tan δ of $S_XT_YD_Z$ gradually increases, and the $S_XT_YD_Z$ polymers tend to be more viscous (Fig. 3h, S43, S44 and Table S13).[67] Considering the dynamic nature of the disulfide bonds and the viscosity of $S_1T_2D_1$, its self-healing behavior was evaluated at 40 °C using an optical microscope (Fig. S45). As shown in Fig. S46, the signals of the sulfur radicals become stronger because heat accelerates their generation. Under heating conditions, the mobility of the polymer chains increases more rapidly and the rate of disulfide bond exchange increases, thereby enabling complete self-healing within 3–4 h.[68,69] In summary, this TA-initiated strategy not only successfully overcomes the processing difficulties of inverse vulcanization polymers (for example, the S_1D_1 polymer in this work) but also greatly improved both the mechanical properties and recyclability of $S_XT_YD_Z$.

3.6 Adhesion properties of $S_XT_YD_Z$

Compared to oxygen-containing compounds, sulfur-containing compounds serve as "polar hydrophobic" hydrogen bonding motifs with the N–H protons of thiourea exhibiting less exchange with water, thereby enabling such compounds to be developed into robust underwater adhesives.[70] However, it is difficult for inverse vulcanization polymers to form effective interactions with substrates due to their low polarity and poor cohesive strength, thereby limiting their application in adhesives.[71,72] The synthesized $S_XT_YD_Z$ polymers have good toughness, and their side chains contain carboxyl groups that can interact with polar groups on the substrate through hydrogen bonding.[73] Additionally, the hydrophobicity exhibited by the polysulfide chains and benzene ring structures in the $S_XT_YD_Z$ polymer backbone allows for the exclusion of interfacial water under humid environments.[74]

To evaluate the adhesive performance of $S_XT_YD_Z$ following TA modification, we conducted adhesion tests through a hot-melt method and lap shear tests using the tensile machine (Fig. S47). We first established three groups of control experiments, including S_1T_1 (1.153 MPa), S_1D_1 (0.605 MPa), and T_1D_1 (0.127 MPa), all of which exhibited weak adhesive strength (Fig. S48). Among the three control groups, T_1D_1 shows stickiness and can easily form interfacial interactions with the substrate, while S_1D_1 exhibits brittleness with good cohesive strength compared to T_1D_1. However, the $S_XT_YD_Z$ polymers modified with TA appear to have remarkable adhesive properties (3.75–4.55 MPa) and adhesion energy (0.7–1.4 MJ m^{-2}) (Fig. 4b). This can be attributed to the hydrogen bonding between the carboxyl groups and the mechanical topography of the polar substrate. Compared to the control groups, the $S_XT_YD_Z$ polymers show increased cohesive strength and enhanced interfacial interactions, indicating that the TA plays a significant role in the interfacial interaction between the adhesive and the substrate.

Subsequently, we conducted an in-depth investigation into the water contact angle, swelling resistance, and cohesive strength of $S_XT_YD_Z$. We first conducted water contact angle experiments on the $S_XT_YD_Z$ polymers. The water contact angle test revealed that both $S_1T_1D_1$ and $S_2T_1D_1$ are hydrophobic, which can be attributed to the hydrophobic polysulfide chains and benzene ring structures in their backbones (Fig. 4c). After immersing the $S_XT_YD_Z$ polymers in UP water for 21 days, we found that the maximum swelling ratio reached only 1.5% of the original weight of the $S_XT_YD_Z$ polymers (Fig. 4d). Additionally, SEM tests were conducted to characterize the surface condition of the $S_XT_YD_Z$ after immersion in water for 21 days. It was found that the surface of $S_1T_2D_1$ had already cracked, while the surfaces of $S_2T_1D_1$ and $S_1T_1D_1$ remained smooth (Fig. S49). This indicates that a high content of hydro-

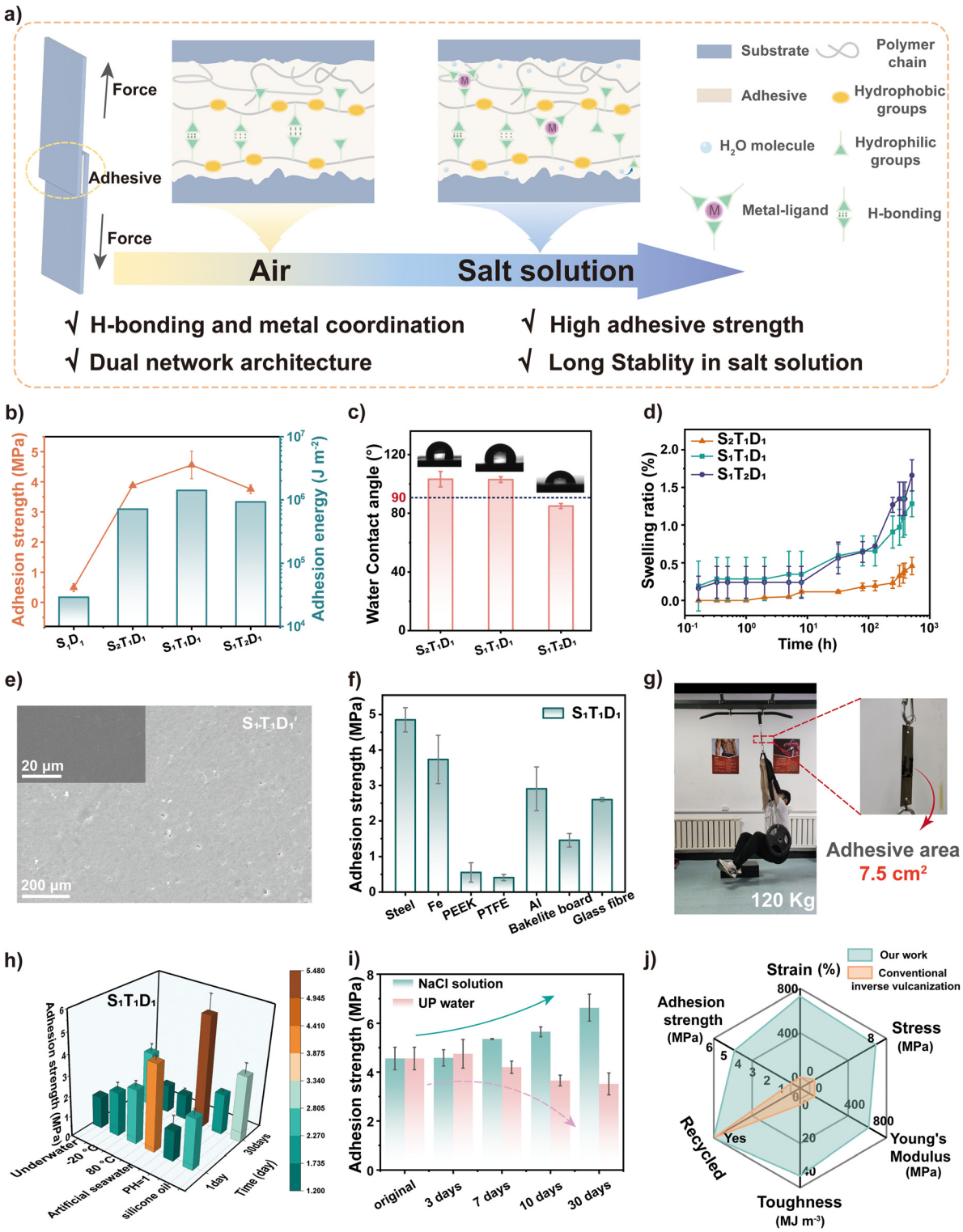

Fig. 4 Adhesion behavior of $S_XT_YD_Z$. (a) Interaction mechanism of $S_XT_YD_Z$ with the substrate. (b) Adhesive strength of $S_XT_YD_Z$ and its control S_1D_1 at RT. (c) Water contact angle of $S_XT_YD_Z$. (d) Swelling behavior of $S_XT_YD_Z$ in UP water at 25 °C. (e) SEM image of $S_1T_1D_1$ following a 21-day immersion. (f) Adhesive strength of $S_1T_1D_1$ on different substrates. (g) Photograph illustrating the bonded two steel base plates capable of withstanding a load of 120 kg (approximately 1176 N). (h) Adhesive strength measurements of $S_1T_1D_1$ in different environments after one day and thirty days. (i) Adhesive strength measurements of $S_1T_1D_1$ immersed in saturated NaCl solution and UP water at different time intervals. (j) Radar chart depicting a comparison of the mechanical and adhesive properties of the conventional inverse vulcanization polymer and $S_1T_1D_1$ of our work.

phobic structures such as sulfur chains and benzene rings in $S_XT_YD_Z$ polymers can more effectively repel water and provide superior cohesive strength (Fig. 4a).

Additionally, SEM analysis was also conducted to characterize the morphology of the $S_XT_YD_Z$ after adhesion failure, and it was found that the surfaces of $S_2T_1D_1$ and $S_1T_2D_1$ exhibited protrusions (Fig. 4e and S50). These protrusions may be produced by insufficient interaction between the adhesion layer and the interface when subjected to external forces, whereas $S_1T_1D_1$ does not show any protrusions. Therefore, we selected $S_1T_1D_1$, which exhibits excellent hydrophobicity and high bond strength, for the subsequent bonding test using different substrates and harsh environments. We conducted lap shear tests on $S_1T_1D_1$ with different substrate materials and evaluated its load-bearing capacity on stainless steel samples with a 7.5 cm^2 adhesive area (Fig. 4f and g). $S_1T_1D_1$ was able to bear a weight of 120 kg, demonstrating excellent load-bearing performance.

Long-term resistance to harsh environments is an important indicator for evaluating adhesive performance. Therefore, we conducted adhesion tests using $S_1T_1D_1$ under various harsh conditions, including at temperatures of −20 °C and 80 °C and in artificial seawater and strong acid environments (Table S15). We found that $S_1T_1D_1$ maintained good adhesive properties (Fig. 4h). Notably, after 30 days of immersion in artificial seawater, the bond strength showed a significant enhancement from 4.24 ± 0.19 MPa to 5.46 ± 0.85 MPa. Owing to the strong adhesive strength of $S_1T_1D_1$, it was not possible to effectively test the glass substrate. Additionally, we placed $S_1T_1D_1$ in saturated saltwater for an underwater load-bearing experiment. The $S_1T_1D_1$ adhesive has been bearing weight for more than 130 days without any fracture (Fig. S51).

Considering the bonding performance enhancement of $S_1T_1D_1$ in artificial seawater, we speculated that the carboxyl groups of the side chains of $S_1T_1D_1$ may coordinate with metal ions, thereby improving the cohesive strength of the $S_1T_1D_1$ polymer and its interfacial interactions with the substrate, thus maintaining long-term stability under underwater load-bearing conditions in a salt solution. To verify our hypothesis, we designed a control experiment by immersing $S_1T_1D_1$ in both UP water and saturated NaCl solution to test its adhesive strength at different time intervals. As shown in Fig. 4i, the adhesive strength of the $S_1T_1D_1$ decreases upon immersion in UP water, whereas a significant increase is observed in the saturated NaCl solution. This observation indicates that $S_1T_1D_1$ may achieve metal coordination enhancement in salt solutions, thereby realizing long-term stability in saline environments. Ultimately, we compiled recent studies on the tensile and adhesion strength of polysulfides and compared the conventional inverse vulcanization S_1D_1 control with our work (Fig. 4j and Table S17), and the $S_XT_YD_Z$ polymers of our work were found to show outstanding adhesive and mechanical properties. We believe that the $S_XT_YD_Z$ polymers can serve as advanced adhesive materials in the field of sulfur-containing polymers.

4. Conclusions

In summary, by modifying the conventional inverse vulcanization of S_1D_1 with TA, we achieved thermoplastic polymers ($S_XT_YD_Z$) with short sulfur rank and improved mechanical properties for humid adhesion. TA can initiate the ROP of S_8 at 120 °C and insert into the polysulfide chain, forming the STA chain with an alternating arrangement of PTA and S atoms, in contrast to the chaotic, long, and disordered sulfur chain in S_1D_1. Compared to the control S_1D_1, which is a brittle and difficult to process, the $S_2T_1D_1$ polymer exhibits good mechanical properties (8.5 MPa) and enhanced recyclability (8.48–11.64 MPa). Crucially, the carboxyl groups confer exceptional humid adhesion stability in saline environments for 130 d *via* metal ion coordination, enhancing cohesive strength. The formulation of these polymers paves the way for the efficient and clean utilization of elemental sulfur, driving sustainable progress in the development of sulfur-containing polymers.

Author contributions

Tongye Zhang: methodology, formal analysis, data curation, writing-original draft. Zhiyue Fang: formal analysis. Shifang Luan: project administration, funding acquisition. Lei Wang: writing-review & editing, supervision, conceptualization. Hengchong Shi: conceptualization, project administration, funding acquisition.

Conflicts of interest

The authors declare that they have no conflicts of interest.

Data availability

The data supporting this article have been included as part of the SI. See DOI: **https://doi.org/10.1039/d5py00658a**.

Acknowledgements

This work is supported by the National Natural Science Foundation of China (Grant No. 52373049), Scientific and Technological Development Program of Jilin Province (Grant No. 20240305045YY), and the Chinese Academy of Sciences-Wego Group Hightech Research & Development Program. The authors would like to thank Xinghong Zhang of the Department of Polymer Science and Engineering of Zhejiang University for helpful discussions on topics related to this work. The authors are also very grateful to Donghua Xu of the State Key Laboratory of Polymer Science and Technology, Changchun Institute of Applied Chemistry, Chinese Academy of Sciences. The authors extend their gratitude to the Shiyanjia Lab (**https://www.shiyanjia.com**) for providing invaluable assistance with the XPS and EPR analysis.

References

1 J. Lim, J. Pyun and K. Char, *Angew. Chem.*, 2015, **127**, 3298–3308.
2 S. T. Ota and G. L. Richmond, *J. Am. Chem. Soc.*, 2011, **133**, 7497–7508.
3 Y. Zhang, R. S. Glass, K. Char and J. Pyun, *Polym. Chem.*, 2019, **10**, 4078–4105.
4 J. Lim, J. Pyun and K. Char, *Angew. Chem., Int. Ed.*, 2015, **54**, 3249–3258.
5 J. J. Griebel, R. S. Glass, K. Char and J. Pyun, *Prog. Polym. Sci.*, 2016, **58**, 90–125.
6 S. Luo, N. Wang, Y. Pan, B. Zheng, F. Li and S. Dong, *Small*, 2024, **20**, e2310839.
7 S. Penck, M. Cypryk, J. Pretula, K. Kaluzynski and P. Lewinski, *Prog. Polym. Sci.*, 2024, **152**, 101818.
8 M. J. H. Worthington, R. L. Kucera and J. M. Chalker, *Green Chem.*, 2017, **19**, 2748–2761.
9 W. J. Chung, J. J. Griebel, E. T. Kim, H. Yoon, A. G. Simmonds, H. J. Ji, P. T. Dirlam, R. S. Glass, J. J. Wie, N. A. Nguyen, B. W. Guralnick, J. Park, Á. Somogyi, P. Theato, M. E. Mackay, Y.-E. Sung, K. Char and J. Pyun, *Nat. Chem.*, 2013, **5**, 518–524.
10 M. Lee, Y. Oh, J. Yu, S. G. Jang, H. Yeo, J.-J. Park and N.-H. You, *Nat. Commun.*, 2023, **14**, 2866.
11 J. J. Griebel, S. Namnabat, E. T. Kim, R. Himmelhuber, D. H. Moronta, W. J. Chung, A. G. Simmonds, K. J. Kim, J. van der Laan, N. A. Nguyen, E. L. Dereniak, M. E. Mackay, K. Char, R. S. Glass, R. A. Norwood and J. Pyun, *Adv. Mater.*, 2014, **26**, 3014–3018.
12 J. J. Griebel, S. Namnabat, E. T. Kim, R. Himmelhuber, D. H. Moronta, W. J. Chung, A. G. Simmonds, K.-J. Kim, J. van der Laan, N. A. Nguyen, E. L. Dereniak, M. E. Mackay, K. Char, R. S. Glass, R. A. Norwood and J. Pyun, *Adv. Mater.*, 2014, **26**, 3014–3018.
13 J. Zhou, M. L. Holekevi Chandrappa, S. Tan, S. Wang, C. Wu, H. Nguyen, C. Wang, H. Liu, S. Yu, Q. R. S. Miller, G. Hyun, J. Holoubek, J. Hong, Y. Xiao, C. Soulen, Z. Fan, E. E. Fullerton, C. J. Brooks, C. Wang, R. J. Clément, Y. Yao, E. Hu, S. P. Ong and P. Liu, *Nature*, 2024, **627**, 301–305.
14 W. Cao, F. Dai, R. Hu and B. Z. Tang, *J. Am. Chem. Soc.*, 2019, **142**, 978–986.
15 T. Tian, R. Hu and B. Z. Tang, *J. Am. Chem. Soc.*, 2018, **140**, 6156–6163.
16 Y. Onose, Y. Ito, J. Kuwabara and T. Kanbara, *Polym. Chem.*, 2022, **13**, 5486–5493.
17 K. Orme, A. H. Fistrovich and C. L. Jenkins, *Macromolecules*, 2020, **53**, 9353–9361.
18 J. Jia, J. Liu, Z.-Q. Wang, T. Liu, P. Yan, X.-Q. Gong, C. Zhao, L. Chen, C. Miao, W. Zhao, S. Cai, X.-C. Wang, A. I. Cooper, X. Wu, T. Hasell and Z.-J. Quan, *Nat. Chem.*, 2022, **14**, 1249–1257.
19 P. Yan, W. Zhao, F. McBride, D. Cai, J. Dale, V. Hanna and T. Hasell, *Nat. Commun.*, 2022, **13**, 4824.
20 H. Yang, J. Huang, Y. Song, H. Yao, W. Huang, X. Xue, L. Jiang, Q. Jiang, B. Jiang and G. Zhang, *J. Am. Chem. Soc.*, 2023, **145**, 14539–14547.
21 D. Wang, Z. Tang, Y. Liu and B. Guo, *Green Chem.*, 2020, **22**, 7337–7342.
22 J. Y. Chao, T. J. Yue, B. H. Ren, G. G. Gu, X. B. Lu and W. M. Ren, *Angew. Chem., Int. Ed.*, 2022, **61**, e202115950.
23 J. M. M. Pople, T. P. Nicholls, L. N. Pham, W. M. Bloch, L. S. Lisboa, M. V. Perkins, C. T. Gibson, M. L. Coote, Z. Jia and J. M. Chalker, *J. Am. Chem. Soc.*, 2023, DOI: **10.1021/jacs.3c03239**.
24 J. Zhang, Q. Zang, F. Yang, H. Zhang, J. Z. Sun and B. Z. Tang, *J. Am. Chem. Soc.*, 2021, **143**, 3944–3950.
25 W. Cao, F. Dai, R. Hu and B. Z. Tang, *J. Am. Chem. Soc.*, 2020, **142**, 978–986.
26 D. H. Kim, W. Jang, K. Choi, J. S. Choi, J. Pyun, J. Lim, K. Char and S. G. Im, *Sci. Adv.*, 2020, **6**, eabb5320.
27 J. Kuwabara, K. Oi, M. M. Watanabe, T. Fukuda and T. Kanbara, *ACS Appl. Polym. Mater.*, 2020, **2**, 5173–5178.
28 L. J. Dodd, Ö. Omar, X. Wu and T. Hasell, *ACS Catal.*, 2021, **11**, 4441–4455.
29 K.-S. Kang, A. Phan, C. Olikagu, T. Lee, D. A. Loy, M. Kwon, H.-J. Paik, S. J. Hong, J. Bang, W. O. Parker Jr, M. Sciarra, A. R. de Angelis and J. Pyun, *Angew. Chem., Int. Ed.*, 2021, **60**, 22900–22907.
30 B.-J. Lee, C. Zhao, J.-H. Yu, T.-H. Kang, H.-Y. Park, J. Kang, Y. Jung, X. Liu, T. Li, W. Xu, X.-B. Zuo, G.-L. Xu, K. Amine and J.-S. Yu, *Nat. Commun.*, 2022, **13**, 4629.
31 D. Wang, Z. Tang, Z. Wang, L. Zhang and B. Guo, *Polym. Chem.*, 2022, **13**, 485–491.
32 D. Wang, Z. Tang, S. Fang, S. Wu, H. Zeng, A. Wang and B. Guo, *Carbon*, 2021, **184**, 409–417.
33 Y. Huang, Y. Liu, G. Si and C. Tan, *ACS Sustainable Chem. Eng.*, 2024, **12**, 2212–2224.
34 V. S. Wadi, K. K. Jena, K. Halique, B. Rožič, L. Cmok, V. Tzitzios and S. M. Alhassan, *Sci. Rep.*, 2020, **10**, 14924.
35 J. Bao, K. P. Martin, E. Cho, K.-S. Kang, R. S. Glass, V. Coropceanu, J.-L. Bredas, W. O. N. Parker, J. T. Njardarson and J. Pyun, *J. Am. Chem. Soc.*, 2023, **145**, 12386–12397.
36 A. Eisenberg and A. V. Tobolsky, *J. Polym. Sci.*, 2003, **46**, 19–28.
37 A. V. Tobolsky, *J. Polym. Sci., Polym. Symp.*, 2007, **12**, 71–78.
38 Q. Laurent, N. Sakai and S. Matile, *Helv. Chim. Acta*, 2019, **102**, e1800209.
39 A. D. Clauss, S. F. Nelsen, M. Ayoub, J. W. Moore, C. R. Landis and F. Weinhold, *Chem. Educ. Res. Pract.*, 2014, **15**, 417–434.
40 Z. Wang, D. Chen, H. Wang, S. Bao, L. Lang, C. Cui, H. Song, J. Yang and W. Liu, *Adv. Mater.*, 2024, **36**, 2404297.
41 K. R. Albanese, P. T. Morris, J. Read de Alaniz, C. M. Bates and C. J. Hawker, *J. Am. Chem. Soc.*, 2023, **145**, 22728–22734.
42 K.-X. Hou, S.-P. Zhao, D.-P. Wang, P.-C. Zhao, C.-H. Li and J.-L. Zuo, *Adv. Funct. Mater.*, 2021, **31**, 2107006.

43 Y. Deng, Q. Zhang, B. L. Feringa, H. Tian and D. H. Qu, *Angew. Chem., Int. Ed.*, 2020, **59**, 5278–5283.
44 C. Chen, X. Yang, S.-J. Li, C. Zhang, Y.-N. Ma, Y.-X. Ma, P. Gao, S.-Z. Gao and X.-J. Huang, *Green Chem.*, 2021, **23**, 1794–1804.
45 Q. Zhang, D.-H. Qu, B. L. Feringa and H. Tian, *J. Am. Chem. Soc.*, 2022, **144**, 2022–2033.
46 L. Packer, E. H. Witt and H. J. Tritschler, *Free Radical Biol. Med.*, 1995, **19**, 227–250.
47 J. Huang, A. A. Wróblewska, J. Steinkoenig, S. Maes and F. E. Du Prez, *Macromolecules*, 2021, **54**, 4658–4668.
48 Z. Fang, L. Wang, C. Liang, J. Qiu, T. Zhang, D. Xu, D. Qi, S. Luan and H. Shi, *Adv. Funct. Mater.*, 2025, **35**, 2418583.
49 A. Khan, R. R. Kisannagar, C. Gouda, D. Gupta and H.-C. Lin, *J. Mater. Chem. A*, 2020, **8**, 19954–19964.
50 S. Pal, J. Shin, K. DeFrates, M. Arslan, K. Dale, H. Chen, D. Ramirez and P. B. Messersmith, *Science*, 2024, **385**, 877–883.
51 P. T. Morris, K. Watanabe, K. R. Albanese, G. T. Kent, R. Gupta, M. Gerst, J. Read de Alaniz, C. J. Hawker and C. M. Bates, *J. Am. Chem. Soc.*, 2024, **146**, 30662–30667.
52 X. Wei, X. Zhang, T. Chen, J. Huang, T. Li, X. Zhang, S. Wang and W. Dong, *ACS Macro Lett.*, 2024, **13**, 1112–1118.
53 L. Wang, K. Yue, Q. Qiao, Z. Zhao, Y. Xu, L. Pan, Y. Liu, H. Li and B. Zhu, *Adv. Energy Mater.*, 2024, **15**, 2402617.
54 Z. Sun, Q. Ou, C. Dong, J. Zhou, H. Hu, C. Li and Z. Huang, *Exploration*, 2024, **4**, 20220167.
55 X.-Y. Hao, B. Yu, L. Li, H. Ju, M. Tian and P.-F. Cao, *Macromolecules*, 2024, **57**, 5063–5072.
56 L. J. Dodd, *RSC Appl. Polym.*, 2025, **3**, 10–42.
57 Y. Deng, Z. Huang, B. L. Feringa, H. Tian, Q. Zhang and D.-H. Qu, *Nat. Commun.*, 2024, **15**, 3855.
58 S. P. O. Danielsen, H. K. Beech, S. Wang, B. M. El-Zaatari, X. Wang, L. Sapir, T. Ouchi, Z. Wang, P. N. Johnson, Y. Hu, D. J. Lundberg, G. Stoychev, S. L. Craig, J. A. Johnson, J. A. Kalow, B. D. Olsen and M. Rubinstein, *Chem. Rev.*, 2021, **121**, 5042–5092.
59 J. Zhang, M. Wang, X. Yao, J. Liu and B. Yan, *ACS Appl. Mater. Interfaces*, 2024, **16**, 54685–54692.
60 M. Huang, L. Liu, W. Guo, L. Cui, G. Gao, Q. Zhang and X. Liu, *Adv. Funct. Mater.*, 2025, **35**, 2413542.
61 S. Yu, Z. Tang, D. Wang, B. Guo and L. Zhang, *Macromolecules*, 2024, **57**, 10120–10129.
62 J. J. Dale, S. Petcher and T. Hasell, *ACS Appl. Polym. Mater.*, 2022, **4**, 3169–3173.
63 J. J. Dale, J. Stanley, R. A. Dop, G. Chronowska-Bojczuk, A. J. Fielding, D. R. Neill and T. Hasell, *Eur. Polym. J.*, 2023, **195**, 112198.
64 C. W. H. Rajawasam, O. J. Dodo, M. A. S. N. Weerasinghe, I. O. Raji, S. V. Wanasinghe, D. Konkolewicz and N. De Alwis Watuthanthrige, *Polym. Chem.*, 2024, **15**, 219–247.
65 M. A. S. N. Weerasinghe, O. J. Dodo, C. W. H. Rajawasam, I. O. Raji, S. V. Wanasinghe, D. Konkolewicz and N. De Alwis Watuthanthrige, *Polym. Chem.*, 2023, **14**, 4503–4514.
66 P. Yan, W. Zhao, S. J. Tonkin, J. M. Chalker, T. L. Schiller and T. Hasell, *Chem. Mater.*, 2022, **34**, 1167–1178.
67 J. J. Griebel, N. A. Nguyen, S. Namnabat, L. E. Anderson, R. S. Glass, R. A. Norwood, M. E. Mackay, K. Char and J. Pyun, *ACS Macro Lett.*, 2015, **4**, 862–866.
68 C. Cui, F. Wang, X. Chen, T. Xu, Z. Li, K. Chen, Y. Guo, Y. Cheng, Z. Ge and Y. Zhang, *Adv. Funct. Mater.*, 2024, **34**, 2315469.
69 X. Xue, C. Li, X. Yu, K. Chenchai, X. Zhang, X. Zhang, G. Zhang and D. Zhang, *Angew. Chem., Int. Ed.*, 2025, **64**, e202425172.
70 K. Kikkawa, Y. Sumiya, K. Okazawa, K. Yoshizawa, Y. Itoh and T. Aida, *J. Am. Chem. Soc.*, 2024, **146**, 21168–21175.
71 H. Huang, S. Zheng, J. Luo, L. Gao, Y. Fang, Z. Zhang, J. Dong and N. Hadjichristidis, *Angew. Chem., Int. Ed.*, 2024, **63**, e202318919.
72 Y. Jin, Z. Wang, C. Hu, J. Wang, K. Yan, J. He, Z. Wang, Z. Wang and L. Yuan, *Green Chem.*, 2023, **25**, 1157–1168.
73 C. Cui, L. Mei, D. Wang, P. Jia, Q. Zhou and W. Liu, *Nat. Commun.*, 2023, **14**, 7707.
74 B. Cheng, J. Yu, T. Arisawa, K. Hayashi, J. J. Richardson, Y. Shibuta and H. Ejima, *Nat. Commun.*, 2022, **13**, 1892.